

Seismic modeling study of the Earth's deep crust

José M. Carcione*, Iclilio R. Finetti[†], and Davide Gei*

ABSTRACT

We use seismic modeling methods to validate the interpretation of deep-crust seismic exploration. An approximation of the stacked section is obtained with the nonreflecting wave equation and the exploding-reflector approach. Using this technique and ray-tracing algorithms, we obtain a geological model by comparing the synthetic section with the real stacked section. An isotropic constitutive equation is assumed in this phase. The exact synthetic stacked section is then obtained by applying the standard processing sequence to a set of synthetic common-shot profiles computed with the variable-density acoustic wave equation. We introduce elliptical P-wave anisotropy and the effects of small-scale inhomogeneities by using a von Kármán autocovariance probability function that simulates scattering Q effects. Verification of the geological model by poststack migration constitutes an additional test. The methodology, which is suitable for areas of complex geology, is applied to a seismic line acquired in the northern Apennines as part of the Italian deep-crust exploration project, CROP. This area is particularly difficult to interpret because of the presence of a complex tectonic setting.

INTRODUCTION

The objective of seismic numerical modeling is to predict the seismogram that a set of sensors would record, given an assumed structure of the subsurface. It is a valuable tool for seismic interpretation and an essential part of seismic inversion algorithms. It is also used to provide data for testing processing algorithms and for evaluating acquisition parameters and processing options for various targets of interests before field data acquisition (Özdenvar et al., 1996).

Seismic modeling has been used for hydrocarbon exploration problems (Kang and McMechan, 1990; Fagin, 1992),

for earthquake seismology problems (Priolo, 1999), and for crustal studies (Yarnold, et al., 1993; Morgante, 1998; Morgante et al., 1998). Modeling synthetic seismograms may then have different purposes. In exploration geophysics, for instance, it is important to perform a sensitivity analysis related to the detectability of a petrophysical variable, such as porosity, fluid type, or fluid saturation. In earthquake seismology the scale of the investigation can be of the order of kilometers for site-response problems (Priolo, 1999) or of the order of tens of kilometers for deep crustal studies (Ponziani et al., 1995). We develop a methodology to validate the seismic response of the Earth's crust on a large-scale basis for the purpose of verifying the main geological features of the upper and lower crusts obtained during the interpretation process.

The interpretation of large-scale structures of the deep crust is mainly based on P-wave information [examples of seismic data are from the Italian CROP and the German DEKORP deep-crust exploration projects (Finetti, 1994; Piali et al., 1998; Rabbel and Gajewski, 1999)]. The source and acquisition parameters for the CROP-03 seismic survey are given in Table 1 [Bertelli and Mazzotti (1998); see also Mazzotti et al. (2000) for alternative parameters]. The survey has been interpreted by Finetti et al. (2001). Amplitude information is relatively important, but a precise determination of the interval velocities is difficult because the residual NMO of reflection events beyond 4–5 s becomes very small. Additional problems are the complex tectonic regime and rough topography with outcrops of high-velocity layers. Moreover, the data are usually of low S/N ratio, thus invalidating the use of techniques such as prestack depth migration. Therefore, we should deal with almost zero-offset P-wave data, and the model design should be based on the stacked time section: well data are scarce, and only oil exploration wells down to 4 km depth are available. The data generally show a rather scarce reflectivity and diffractions, which may reveal the presence of fault planes. On the basis of these facts, it is unrealistic to use sophisticated modeling techniques. Therefore, we do not consider mode conversion (i.e., S-waves) and intrinsic attenuation, which, in this situation, constitute second-order effects. Anisotropic effects on the P-wave are modeled with an

Manuscript received by the Editor July 6, 2001; revised manuscript received April 11, 2002.

*Istituto Nazionale di Oceanografia e di Geofisica Sperimentale (OGS), Borgo Grotta Gigante 42c, 34010 Sgonico, Trieste, Italy. E-mail: jcarcione@ogs.trieste.it; dgei@ogs.trieste.it.

[†]University of Trieste Exploration Geophysics Group (EGG), Department of Geological, Environmental and Marine Sciences, via Weiss 1-34127, Trieste, Italy.

© 2003 Society of Exploration Geophysicists. All rights reserved.

elliptical anisotropic rheology since anisotropy can be important in the upper mantle (Guest and Thomson, 1992).

The modeling method is based on the 2-D acoustic wave equation with variable density. This choice allows us to define the acoustic impedance of each macrolayer. For instance, the asthenosphere (from the Greek *asthenos*, meaning “weak”) has a lower P-wave velocity and a slightly lower density than the overlying strata because of the in-situ stress–temperature condition that implies partial melting and ductile behavior (Hales, 1991; Anderson, 1995). Then, the velocity field and density of each stratum can be defined on the basis of the reflector strength and global geological information of the study area. The data are in part degraded by the heterogeneous nature of the crust at small scales. Constraints on the velocity variations of these small-scale heterogeneities can be estimated from P-wave sonic logs. We introduce these inhomogeneities by using a spatially isotropic von Kármán autocovariance probability function of high fractal dimension that simulates scattering Q effects (Frankel and Clayton, 1986; Hurich, 1996; Holliger, 1997). This theory describes in part the seismic attenuation of the crust (Mitchell, 1995). A typical correlation length is 100 m, and the standard deviation of the velocity fluctuations ranges from 200 to 400 m/s.

The simulation of a stacked seismic section requires the calculation of a set of common-shot experiments and application of the standard processing sequence. To reduce computing time, we compute a zero-offset stacked section, with a single simulation, by using the exploding-reflector concept and the so-called nonreflecting wave equation (Baysal et al., 1984; Carcione et al., 1994). This nonphysical modification of the wave equation implies a constant impedance model to avoid multiple reflections, which are, in principle, absent from stacked sections and constitute unwanted artifacts in migration processes. In the exploding-reflector method, each reflection point in the subsurface explodes at $t = 0$ with a magnitude proportional to the normal-incidence reflection coefficient. The nonreflecting equation is a modification of the wave equation, where the impedance is constant over the whole model space. In this way, nonphysical multiple reflections are avoided and the recorded events are primary reflections. The density is used as a free parameter to obtain a constant impedance model and avoid multiple reflections. The reflection strength is then implicit in the source strength. Moreover, the method generates normal-incidence reflections, i.e., those having identical downgoing and upgoing wavepaths. To obtain the two-way

traveltime, the phase velocities are halved. Because of sampling constraints, halving the velocities implies doubling the number of gridpoints. We do not consider anisotropy and scattering in this process. In the final phase of the modeling study, we use the variable-density acoustic wave equation to compute common-shot and common-offset synthetic surveys, which are used to obtain the synthetic stacked time section using the standard processing sequence. The verification of the geological model by poststack migration constitutes an additional test.

The numerical solver consists of the pseudospectral Fourier method for computing the spatial derivatives and a second-order leapfrog method for time integration (Carcione et al., 1994). An averaging method, developed by Zeng and West (1996), reduces spurious diffractions arising from an inappropriate modeling of curved and dipping interfaces (the so-called staircase effect). It is based on a spatially weighted averaging of the model properties.

THE MODELING METHOD

The wave equation

The variable-density wave equation for elliptically anisotropic media is

$$\rho c^2 \frac{\partial}{\partial x} \left(\frac{1}{\rho} \frac{\partial p}{\partial x} \right) + \rho c_3^2 \frac{\partial}{\partial z} \left(\frac{1}{\rho} \frac{\partial p}{\partial z} \right) = \frac{\partial^2 p}{\partial t^2} + f, \quad (1)$$

where $p(x, z, t)$ is the pressure field, $\rho(x, z)$ is the material density, $c(x, z)$ is the horizontal P-wave velocity, $c_3(x, z)$ is the vertical P-wave velocity, and $f(x, z, t)$ is the source. Equation (1) is obtained by substituting the stress-strain relations $-p = \rho c_i^2 \epsilon_i$, $i = 1, 3$, where ϵ_i are the strain components, into Newton's equations, $-\partial_i \rho^{-1} \partial_i p = \ddot{\epsilon}_i$, where ∂_i is the spatial derivative with respect to x ($i = 1$) and z ($i = 3$) and the double dot denotes the second time derivative [see DeSanto (1992, p. 84) for the isotropic version].

Assuming constant material properties, $s = 0$, and substituting the plane-wave kernel $\exp[i\omega(t - s_x x - s_z z)]$, where ω is the angular frequency and s_i are the slowness components, into equation (1), we obtain the dispersion relation

$$\frac{s_x^2}{c^2} + \frac{s_z^2}{c_3^2} = 1. \quad (2)$$

This is an ellipse with semiaxes $1/c$ and $1/c_3$. We assume that the major semiaxis of the ellipse is vertical, that is, $c_3 \leq c$. Seismic anisotropy A is usually reported in percentage terms (e.g., Rudnick and Fountain, 1995):

$$A = 100 \left(1 - \frac{c_3}{c} \right). \quad (3)$$

The isotropic case is obtained for $c_3 \equiv c$.

We consider the source function

$$s(x, z, t) = \delta(x - x_0) \delta(z - z_0) h(t), \quad (4)$$

where δ is Dirac's delta, (x_0, z_0) is the source location, and $h(t)$ is the source time history. To derive the exploding-reflector

Table 1. Source and acquisition parameters of CROP-03 seismic survey.

Source	
Charge weight	15–30 kg
Hole depth	30–40 m
Shot interval	180 m
Shot pattern	Single hole
Seismic line	
Receivers	10-Hz geophones
Receivers per group	24
Number of groups	192
Group spacing	60 m
Minimum offset	30 m
Layout	Split symmetric
Coverage	3200%

isotropic wave equation with the nonreflecting, constant impedance – condition, we assume that the acoustic impedance

$$I = \rho c \quad (5)$$

is constant throughout all of the model space. Using this condition, equation (1) becomes

$$c \frac{\partial}{\partial x} \left(c \frac{\partial p}{\partial x} \right) + c \frac{\partial}{\partial z} \left(c \frac{\partial p}{\partial z} \right) = \frac{\partial^2 p}{\partial t^2} + s \quad (6)$$

(Baysal et al., 1984; Carcione et al., 1994). The normal-incidence reflection coefficient is zero for this equation, and it becomes the constant density wave equation when the velocity is constant.

We place a source on each gridpoint (i, j) defining the interfaces

$$s(x, z, t) = R\delta(x - x_i)\delta(z - z_j)h(t), \quad (7)$$

where R is the normal-incidence reflection coefficient and (x_i, z_j) is the source location. The normal-incidence reflection coefficient R is

$$R = \frac{I_2 - I_1}{I_1 + I_2} \quad (8)$$

(DeSanto, 1992, p. 5), where 1 and 2 denote the upper and lower media.

The source

The time history of the source is

$$h(t) = \exp\left[-\frac{\Delta\omega^2(t - t_0)^2}{4}\right] \cos[\bar{\omega}(t - t_0)]. \quad (9)$$

In the frequency domain,

$$\tilde{h}(\omega) = \frac{\sqrt{\pi}}{\Delta\omega} \left\{ \exp\left[-\left(\frac{\omega + \bar{\omega}}{\Delta\omega}\right)^2\right] + \exp\left[-\left(\frac{\omega - \bar{\omega}}{\Delta\omega}\right)^2\right] \right\} \exp(i\omega t_0), \quad (10)$$

where t_0 is a delay, $\bar{\omega} = \pi f_{\max}$ is the central angular frequency, with f_{\max} the cut-off frequency of the source, and $2\Delta\omega$ is the width of the pulse. Note that the convention for the inverse Fourier transform is $h(t) = \int \tilde{h}(\omega) \exp(-i\omega t) d\omega$.

The source is implemented in one gridpoint in view of the accuracy of the differential operators. Numerically, in 1-D space and uniform grid spacing, the strength of a discrete delta function in the spatial domain is $1/dx$, where dx is the grid size, since each spatial sample is represented by a sinc function with argument $\pi x/dx$ (the spatial integration of this function is precisely dx). The introduction of the discrete delta will alias the wavenumbers beyond the Nyquist (π/dx) to the lower wavenumbers. However, if the source time function $h(t)$ is band-limited, the wavenumbers greater than $k_{\max} = 2\pi f_{\max}/c_{\min}$ will be filtered, where c_{\min} is the minimum phase velocity.

Scattering effects

Let Δc_0 be the maximum deviation of the velocity field from the background value c_0 . The velocity field at (x, z) is first

subjected to the variations $(\Delta c)^r$ such that

$$-\Delta c_0 \leq (\Delta c)^r \leq \Delta c_0, \quad (11)$$

where $(\Delta c)^r$ is obtained from a 2-D random generator and the superindex r denotes random. (Random numbers between 0 and 1 are generated and then scaled to the interval $[-1, 1]\Delta c_0$.)

Small-scale P-wave velocity variations in the lithosphere is well described by the von Kármán autocovariance function (Frankel and Clayton, 1986; Holliger, 1997). The corresponding wavenumber-domain power spectrum is

$$C(k_x, k_z) = K(1 + k^2 a^2)^{-(\nu + N/2)}, \quad (12)$$

where $k = \sqrt{k_x^2 + k_z^2}$ is the wavenumber, a is the correlation length, ν ($0 < \nu < 1$) is a self-similarity coefficient, K is a normalization constant, and N is the Euclidean dimension. The von Kármán correlation function describes self-affine, fractal processes of fractal dimension $N + 1 - \nu$ at scale smaller than a .

The velocity is then calculated as

$$c(x, z) = c_0 \pm \Delta c(x, z), \quad (13)$$

where

$$\tilde{\Delta c}(k_x, k_z) = (\tilde{\Delta c})^r(k_x, k_z)C(k_x, k_z), \quad (14)$$

with $(\tilde{\Delta c})^r(k_x, k_z)$ being the Fourier transform of $(\Delta c)^r(x, z)$. (The tilde denotes the space Fourier transform.)

The numerical method

The spatial derivatives are computed by using the Fourier method. The spectral coefficients are calculated with the fast Fourier transform (FFT), based on a vectorized version of the mixed-radii FFT (Carcione et al., 1994). This differential operator is infinitely accurate up to the Nyquist wavenumber, corresponding to a spatial wavelength of two gridpoints. This means that if the source is band-limited, the algorithm is free of spatial numerical dispersion and aliasing effects, provided that the grid spacing is chosen $dx \leq c_{\min}/(2f_{\max})$.

The time integration of equations (1) and (6) is performed with the following second-order differencing scheme:

$$\dot{p}^{n+\frac{1}{2}} = \dot{p}^{n-\frac{1}{2}} - dt (L\dot{p}^n - s^n) \quad (15)$$

and

$$p^{n+1} = p^n + dt \dot{p}^{n+\frac{1}{2}}, \quad (16)$$

where $t = n dt$, with n a natural number and dt the time step; \dot{p} is the time derivative of the pressure; and L is the differential operator of the left side of the wave equations [e.g., $L = c \partial_x c \partial_x$ in equation (6)].

Because the wave equation is linear, seismograms with different dominant frequencies and time histories can be implemented by convolving $h(t)$ with only one simulation obtained with $\delta(t)$ as a source (a discrete delta with strength $1/dt$).

EXAMPLE: THE ITALIAN DEEP CRUST

The location of the CROP-03 seismic line across the northern Apennines is shown in Figure 1. Crustal settings and evolving

sketches of the studied area are proposed by various authors (D'Offizi et al., 1994; Vai, 1994; Ponziani et al., 1995). A complete innovative reconstruction of the crustal tectonodynamics of the whole northern Apennines, including the subduction of the Alpine Tethys, has been performed by Finetti et al. (2001). According to this reconstruction, the Alpine system began forming in the Upper Cretaceous as a result of the collision between Adria and Europe, with subduction of the Alpine Tethys beneath the Adria plate (see Figures 3 and 7). The northern Apennines mountain chain begun its development in the Late Oligocene–Early Miocene when the Corso-Sardinian block rotated counterclockwise and collided with the Adria plate. A second Apenninic geodynamic stage took place from the Middle–Upper Miocene to the present, with subduction of the Ionian slab, opening of the Tyrrhenian Ocean, and formation of the highest mountains. A time section of line CROP-03 is displayed in Figures 2a and 2b (line drawing; the processing technique is standard). The stronger seismic events are plotted in Figure 2b. The numbers indicate the relative amplitude of the events. The line drawing is, in principle, difficult to determine on the basis of the picture shown in Figure 2a. The identification of the main events is performed on a larger version (1 m × 2 m). Moreover, a semblance-like procedure is used to identify the coherent events and their relative amplitudes (see discussion below). Figure 3 shows an interpretation of part of the seismic section in Figure 2a (Finetti et al., 2001). The events correspond to the major shear plane (*K*), top of the lower crust (*L*), Moho of the Adria plate (*Ma*), top of the subducted slab

of the Alpine Tethys (*O*), and Moho of the subducted Tethyan slab (*Mo*). The *K* horizon in the upper crust corresponds to a shear plane separating the brittle from the ductile crust.

The first phase of the modeling approach is to iteratively use a zero-offset ray-tracing algorithm to obtain the location of the geological interfaces. A first estimation of the seismic velocities is obtained from prior geological and geophysical information of the study area. The P-wave seismic-velocity values are taken from various sources (e.g., Ponziani et al., 1995) and considering the data published by Christensen (1989), Rudnick and Fountain (1995), and Brittan and Warner (1996). A first version of the geological model is shown in Figure 4, where the main zero-offset ray trajectories are indicated. Because of the limitations of the ray-tracing algorithm, structures such as fault planes cannot be simulated.

The zero-offset (stacked) section is approximated by using exploding-reflector simulations. In the exploding-reflector algorithm the source strength is proportional to the reflection coefficient, which is proportional to the acoustic-impedance contrast. Thus, the density of each layer is obtained by using the relative amplitudes indicated in Figure 2b. To obtain these amplitudes, the data have been corrected for geometrical spreading and attenuation (using a quality factor of 100). Then, each event is windowed and the amplitude is obtained as the arithmetic average of the sum of the peak amplitude of the traces. We also consider the values provided by Rudnick and Fountain (1995). Our calculations agree with the gravity model proposed by Larocchi et al. (1998). The mesh has 1200 × 720 points, with a grid spacing of 72 m. To avoid wraparound, absorbing strips 40 gridpoints long are implemented at the boundaries of the numerical mesh. The dominant frequency of the source is 6 Hz, and the wavefield is computed by using a time step of 1 ms.

The geological model is shown in Figure 5 (see Table 2) (anisotropy and scattering effects are not taken into account in this phase). Figure 6 shows the exploding-reflector seismic section. The improvement over the model shown in Figure 4 consists of the inclusion of fault planes based on the presence of diffraction events. The interpreter plays an important role in the phase, integrating prior knowledge of the regional tectonic features (Finetti et al., 2001). Part of the CROP-03 profile is located near a geothermal field where relatively high heat flow and geothermal gradients are expected. However, it is difficult to determine the effects of temperature on the seismic velocities. Typical velocity gradients are 0.05–0.5 (m/s)°C⁻¹ (Brittan and Warner, 1996; Gualtieri and Zappone, 1998). Thus, a difference of 200°C implies velocity changes of 10–100 m/s, which are in many cases less than the experimental error obtained with seismic methods (Brittan and Warner, 1996).

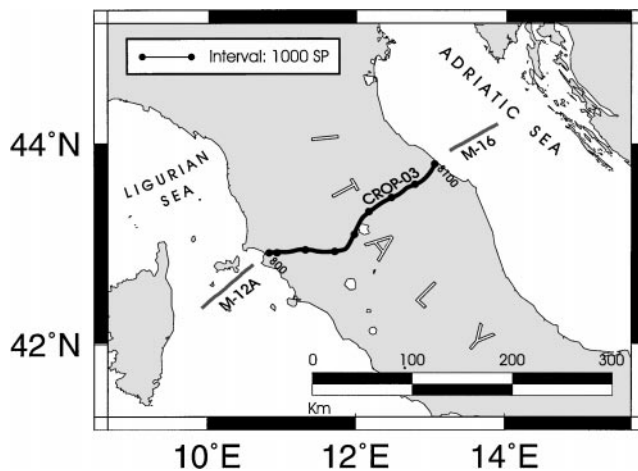


Fig. 1. Location of the CROP-03 seismic line in the northern Apennines.

Table 2. Acoustic properties. P-wave velocities, anisotropy parameter, density, autocorrelation distance, maximum velocity perturbation and fractal number.

Layer	Medium	c (km/s)	A (%)	ρ (g/cm ³)	a (m)	Δc_0 (m/s)	ν
1	Tertiary formations	3.5	0	2.5	—	—	—
2	Tuscan sequence	4.8	0	2.59	—	—	—
3	Triassic evaporites	6.0	0	2.7	—	—	—
4	Batholite	5.0	0	2.55	—	—	—
5	Upper crust	5.8	3	2.67	200	480	0.15
6	Lower crust	6.8	5	2.69	150	420	0.20
7	Upper mantle	8.0	6	3.28	300	640	0.18
8	Oceanic crust	7.0	7	3	—	—	—
9	Asthenosphere	7.8	3	3.18	400	620	0.15

Figure 7 shows the same geological section of Figure 5, with an interpretation of the fault planes on the basis of the preceding information and prior regional geological information (Finetti et al., 2001). This section of the CROP-03 profile shows a compressive deformation system which involves all of the lithospheric units. We distinguish an east-verging compressive regime involving the first three sedimentary layers and part of the upper crust. Below the *K* horizon, we can also see a series of west-verging thrust faults affecting the lower crust and the upper mantle, associated with the co-Alpine stage during the subduction of the Alpine Tethys (Finetti et al., 2001). The *K* horizon, which divides the two opposite fault verging polarities, is a reflector characterized by high amplitude and locally displaying bright-spot features, very likely from fluid saturation.

Eastward-dipping reflectors at about 9 s (two-way traveltime) in the west part of the section—going to about 16 s below CDP 2000—have been identified as the subducted Alpine Tethyan. In the deeper part of the section we identify a few reflections attributed to the asthenosphere.

In the following, we consider anisotropy and scattering effects, according to the values given in Table 2. Since the wavefront is elliptical, the moveout velocity is the velocity for a wave traveling in the horizontal direction, that is, c . This is the velocity obtained from surface measurements (Levin, 1978). Figure 8 shows the perturbation of the velocity field ($\Delta c(x, z)$) of a representative part of the upper mantle. To simulate tenfold CMP acquisition, 100 common shots with 80 split-symmetric channels are computed. The shot interval is 576 m, and the group

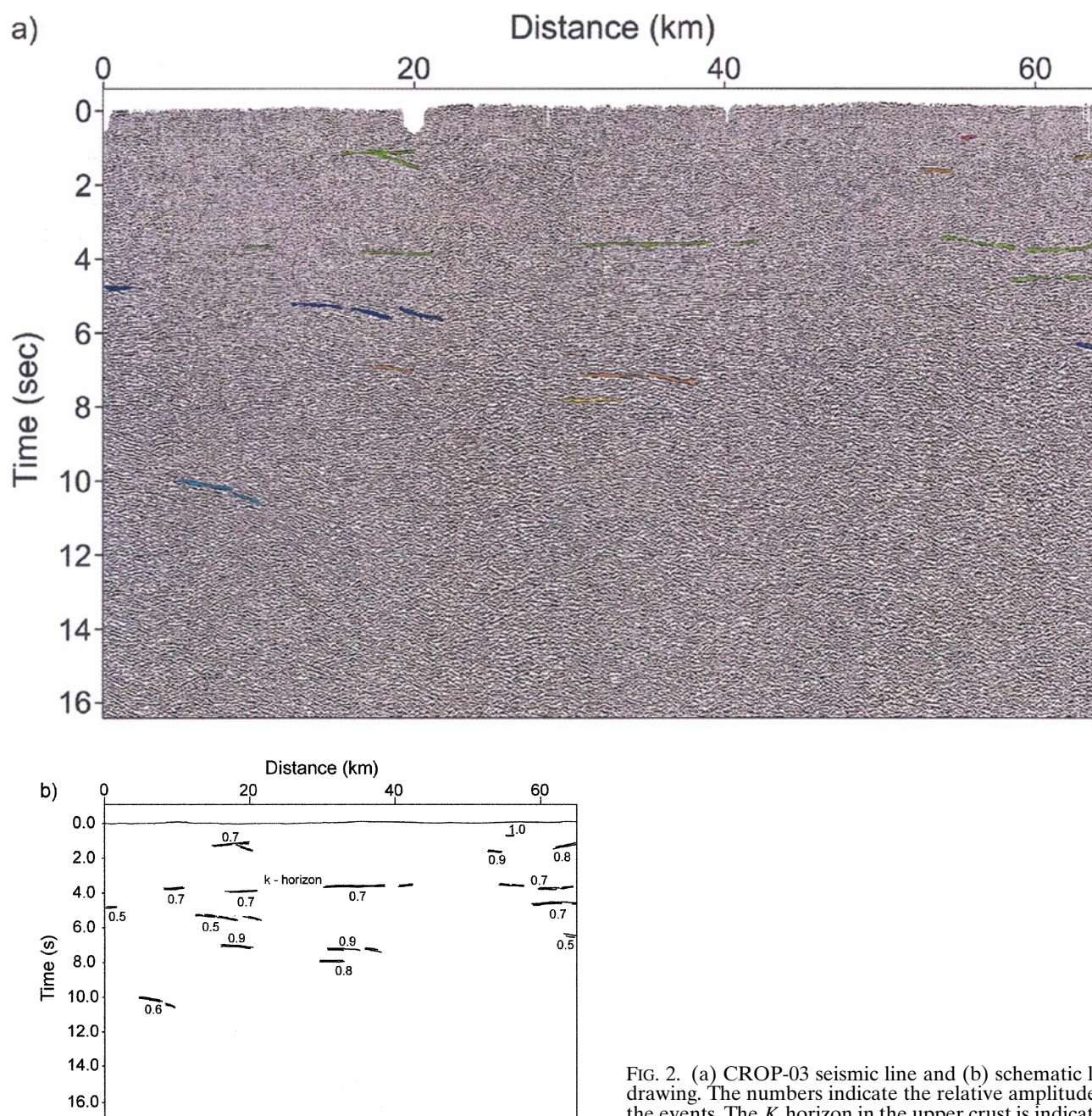


FIG. 2. (a) CROP-03 seismic line and (b) schematic line drawing. The numbers indicate the relative amplitude of the events. The *K* horizon in the upper crust is indicated.

spacing is 144 m. The mesh has 600×360 points, a grid spacing of 144 m, and 40 gridpoints for each absorbing strip. The positions of the first and last shots are $x = 0$ and $x = 60$ km, respectively.

Figure 9 shows a common-shot gather, where the indices denote the reflection events generated at the different interfaces indicated in Figure 5 and 7b. In this case, all of the traces of the numerical mesh are shown in the seismogram. Figure 10 shows two common-offset sections, corresponding to the near (a) and far (b) offsets. They resemble the stacked section—in particular, the near-offset section. The stacked section and its poststacked time migration are displayed in Figures 11a and 11b, respectively. The time migration algorithm uses the interval velocities of the NMO velocity panels. The location of the events in the unmigrated section agree fairly well with the interpretation shown in Figure 3, and the migrated section is in good agreement with the model shown in Figure 7a. Note the migration of the batholite diffraction to a diffraction point (below 17 km) and the removal of the event corresponding to the oceanic slab (layer 8) [this reflector is outside the model (see Figure 7b)]. The results allow us to conclude with confidence that the interpreted events correspond to primary reflections.

CONCLUSIONS

Synthetic seismograms are useful in recognizing patterns associated with different types of structures and predicting some of the drawbacks when interpreting migrated and unmigrated

sections of a given complex structure. We show in this work how to use seismic modeling methods to validate the interpretation of deep-crust seismic sections. The procedure involves the following:

- 1) line drawing to identify the location and strength of the main events,
- 2) ray tracing to generate a first version of the geological model in terms of seismic velocities,

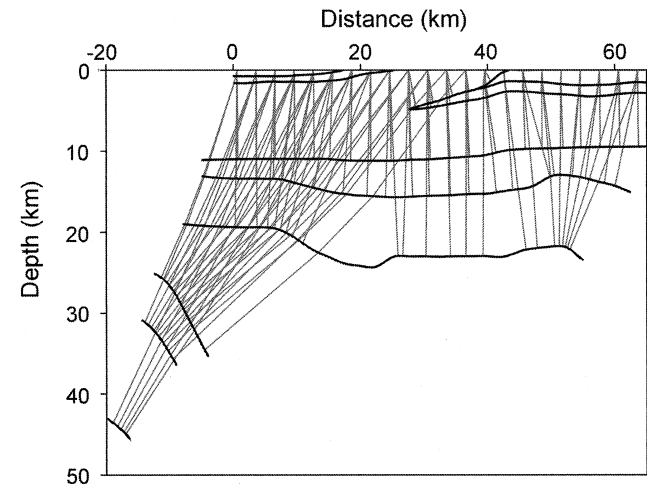


FIG. 4. First version of the geological model obtained from zero-offset ray tracing. The zero-offset raypaths are indicated.

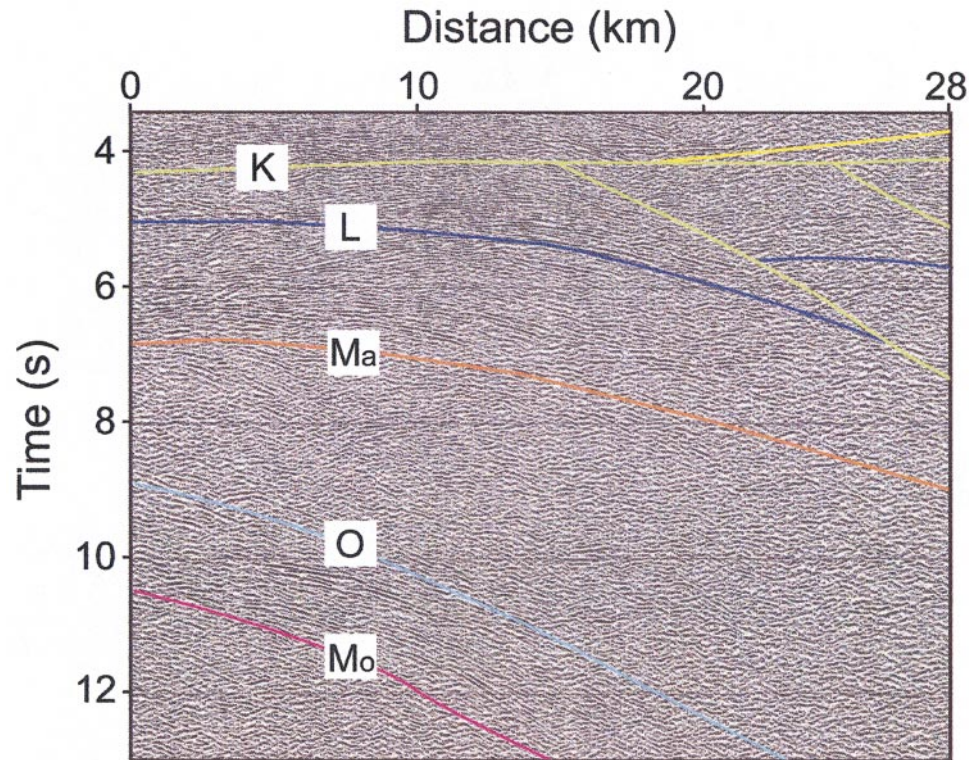


FIG. 3. Interpretation of part of the seismic section shown in Figure 2a (Finetti et al., 2001). The events correspond to the major shear plane (*K*), top of lower crust (*L*), Moho of Adria plate (*Ma*), top of subducted slab of Alpine Tethys (*O*), and Moho of subducted Tethyan slab (*Mo*).

- 3) exploding-reflector experiments to generate a geological model in terms of seismic velocity and mass density (anisotropy and scattering are not considered in this phase),
- 4) refining the model on the basis of prior geological and geophysical information (inclusions of fault planes, etc.), and
- 5) computation of common shots and stacking of the synthetic data to verify the presence of the primary reflections (anisotropy and scattering losses are considered in this phase).

The model is further improved by considering random heterogeneities, which characterize the seismic response of the crust and mantle at different scales. The result is a complete characterization of the geological setting, with the possibility of calculating realistic common-shot seismograms to further investigate and improve the interpretation of the different geological structures.

It is important to point out that the modeling methodology is used to verify the geological model obtained in the interpretation phase. This process relies on the ability and knowledge

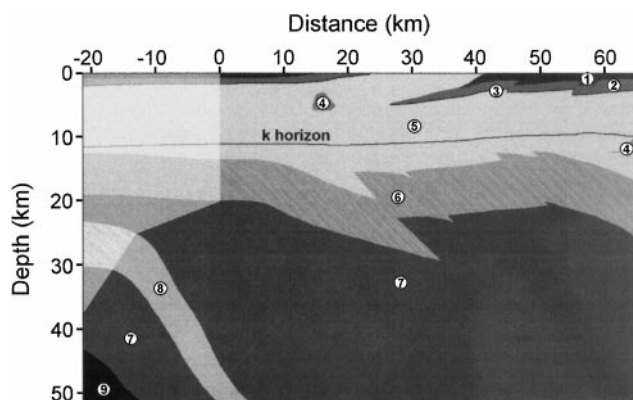


FIG. 5. Geological model in terms of seismic velocity and mass density, used for the exploding-reflector simulations. The numbers refer to layers in Table 2.

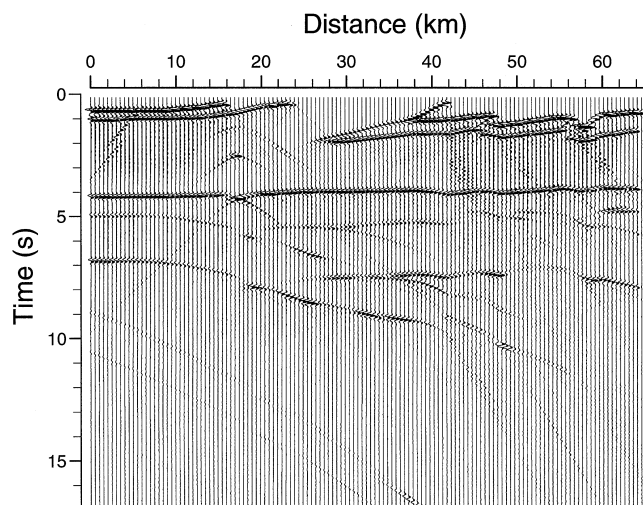


FIG. 6. Exploding-reflector response of the model displayed in Figure 5.

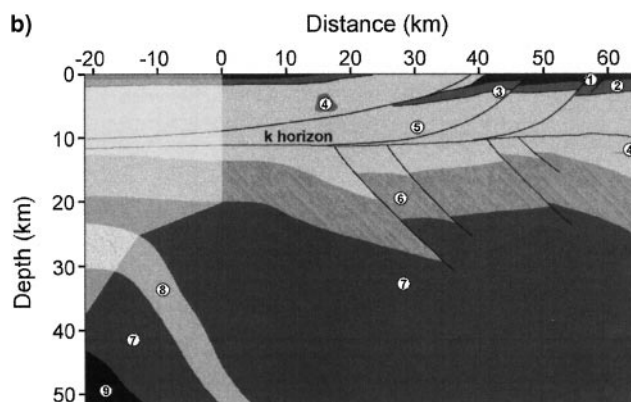
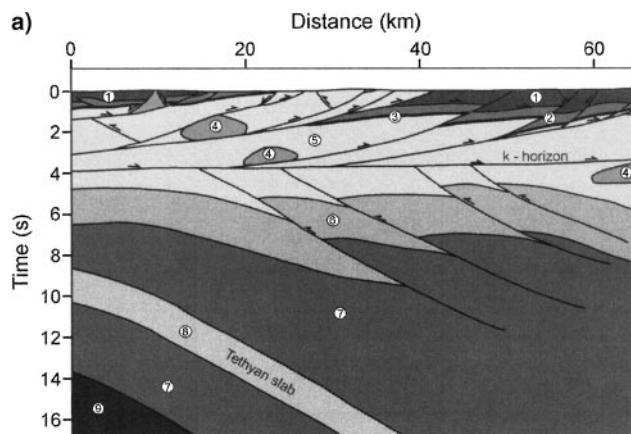


FIG. 7. Seismogeological section, in (a) two-way traveltimes and (b) depth, after a reinterpretation on the basis of ray-tracing results, exploding-reflector simulations, and prior geological information. The numbers refer to the layers in Table 2.

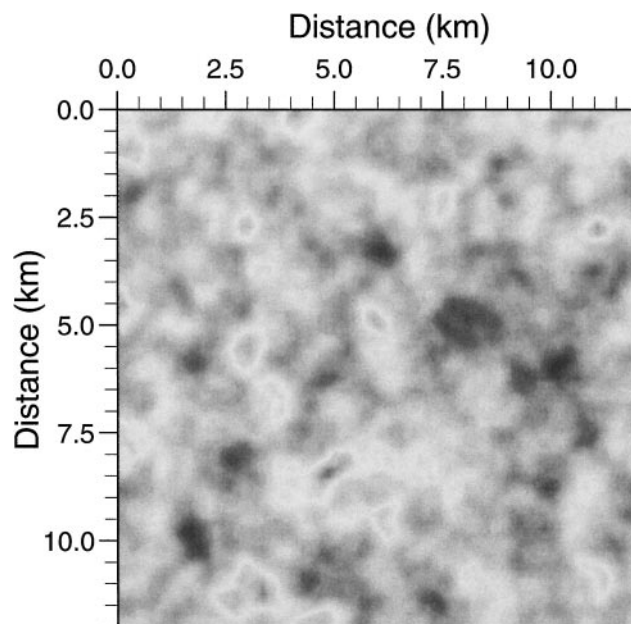


FIG. 8. Velocity field perturbations for part of the upper mantle, obtained from the von Kármán autocovariance function (see Table 2).

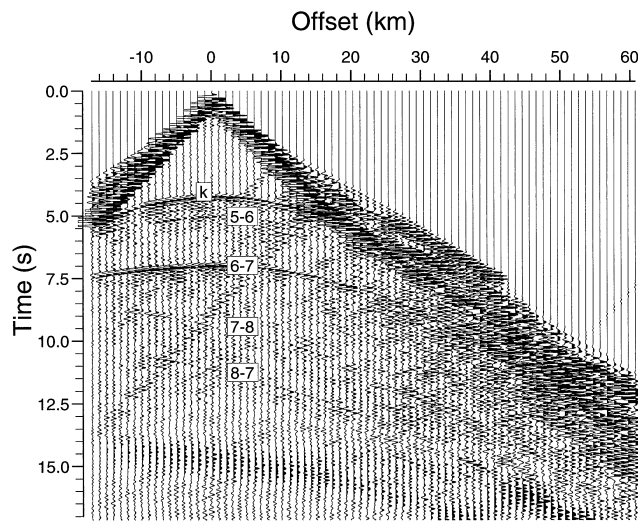


FIG. 9. Common-shot gather corresponding to the model shown in Figure 5. The labels denote the reflection events generated at the interfaces indicated in Figure 7. The source is located at $x = 0$. The numbers refer to the layers in Table 2.

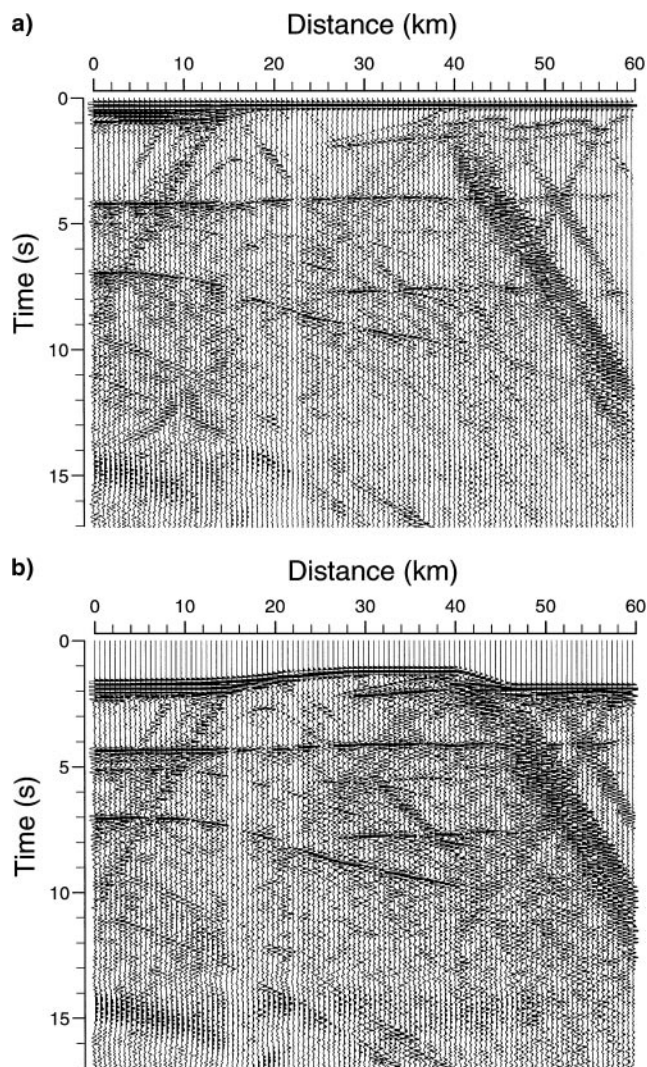


FIG. 10. (a) Near-offset and (b) far-offset sections corresponding to the model shown in Figure 5.

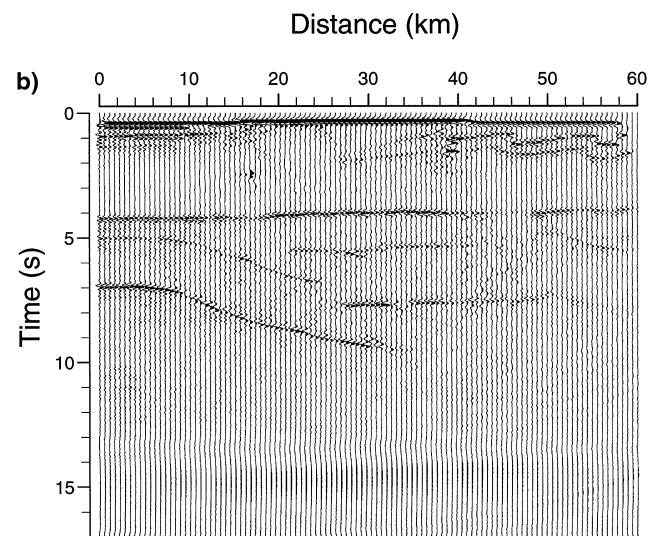
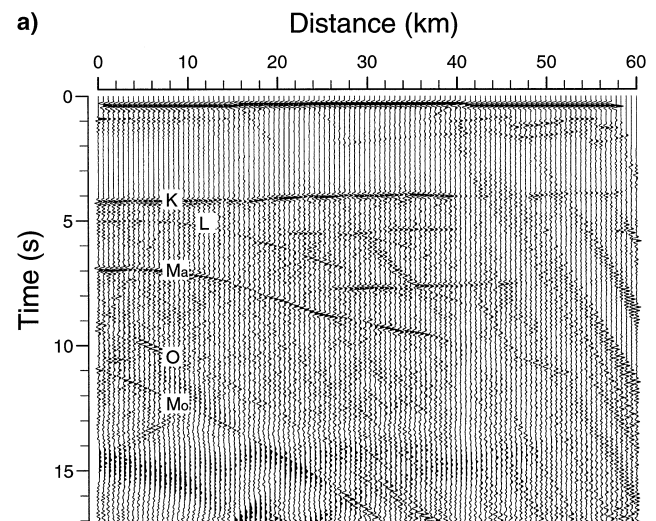


FIG. 11. (a) Stacked and (b) time-migrated sections corresponding to the model shown in Figure 5. These sections give clear evidence of compressive tectonism: east verging above the K horizon and west verging below this reflector. The events correspond to the major shear plane (K), top of lower crust (L), Moho of Adria plate (Ma), top of subducted slab of Alpine Tethys (O), and Moho of subducted Tethyan slab (Mo).

of the interpreter on the basis prior knowledge of the main tectonic characteristics of the study area.

ACKNOWLEDGMENTS

We used Seismic Unix to process the data. This work was funded in part by MURST (Italian Ministry of University, Scientific Research and Technology) under the framework of COFIN-2000 (I.R.F.). We thank one of the reviewers for helpful comments and suggestions to improve this paper. We dedicate this article to the memory of Licio Cernobori.

REFERENCES

- Anderson, D. L., 1995, Lithosphere, asthenosphere and perisphere: *Rev. Geophys.*, **33**, No., 125–149.
 Baysal, E., Kosloff, D. D., and Sherwood, J. W. C., 1984, A two-way nonreflecting wave equation: *Geophysics*, **49**, 132–141.

- Bertelli, L., and Mazzotti, A., 1998, Planning and acquisition of the NVR CROP-03 seismic profile: *Mem. Soc. Geol. It.*, **52**, 9–21.
- Brittan, J., and Warner, M., 1996, Seismic velocity, heterogeneity, and the composition of the lower crust: *Tectonophysics*, **264**, 249–259.
- Carcione, J. M., Böhm, G., and Marchetti, A., 1994, Simulation of a CMP seismic section: *J. Seis. Expl.*, **3**, 381–396.
- Christensen, N. I., 1989, Reflectivity and seismic properties of the deep continental crust: *J. Geophys. Res.*, **94**, No. B12, 17793–17804.
- DeSanto, J. A., 1992, *Scalar wave theory*: Springer-Verlag Berlin.
- D'Offizi, S., Minelli, G., and Piali, G., 1994, Foredeeps and thrust systems in the northern Apennines: *Boll. Geof. Teor. Appl.*, **36**, 91–102.
- Fagin, S. W., 1992, Seismic modeling of geological structures: Applications to exploration problems: *Soc. Expl. Geophys.*
- Finetti, I., Ed., 1994, CROP project, offshore crustal seismic profiling in the central Mediterranean: *Boll. Geof. Teor. Appl.*, **36**, 1–536.
- Finetti, I. R., Boccaletti, M., Bonini, M., Del Ben, A., Geletti, R., Pipan, M., and Sani, F., 2001, Crustal section based on CROP seismic data across the north Tyrrhenian—northern Apennines—Adriatic Sea: *Tectonophysics*, **343**, 135–163.
- Frankel, A., and Clayton, R. W., 1986, Finite difference simulations of seismic scattering: Implications for the propagation of short-period seismic waves in the crust and models of crustal heterogeneity: *J. Geophys. Res.*, **91**, No. B6, 6465–6489.
- Gualtieri, L., and Zappone, A., 1998, Hypothesis of ensialic subduction in the northern Apennines: A petrophysical contribution: *Mem. Soc. Geol. It.*, **52**, 205–214.
- Guest, W. S., and Thomson, C. J., 1992, A source of significant transverse isotropy arrivals from an isotropic-anisotropic interface, e.g., the Moho: *Geophys. J. Internat.*, **111**, 309–318.
- Hales, A. L., 1991, Upper mantle models and the thickness of the continental lithosphere: *Geophys. J. Internat.*, **105**, 355–363.
- Holliger, K., 1997, Seismic scattering in the upper crystalline crust based on evidence from sonic logs: *Geophys. J. Internat.*, **128**, 65–72.
- Hurich, C. A., 1996, Statistical description of seismic reflection wavefields: A step towards quantitative interpretation of deep seismic reflection profiles: *Geophys. J. Internat.*, **125**, 719–728.
- Kang, I. B., and McMechan, G. A., 1990, Two-dimensional elastic pseudo-spectral modeling of wide-aperture seismic array data with application to the Wichita uplift—Anadarko basin region of southwestern Oklahoma: *Bull. Seis. Soc. Am.*, **80**, 1677–1695.
- Larocchi, L., Gualtieri, L., and Cassinis, R., 1998, 2D lithospheric gravity modelling along the CROP-03 profile: *Mem. Soc. Geol. It.*, **52**, 225–230.
- Levin, F., 1978, The reflection, refraction, and diffraction of waves in media with an elliptical velocity dependence: *Geophysics*, **43**, 528–537.
- Mazzotti, A. P., Stucchi, E., Fradelizio, G. L., Zanzi, L., and Scandone, P., 2000, Seismic exploration in complex terrains: A processing experience in the southern Apennines: *Geophysics*, **65**, 1402–1417.
- Mitchell, B. J., 1995, Anelastic structure and evolution of the continental crust and upper mantle from seismic surface wave attenuation: *Rev. Geophys.*, **33**, No. 4, 441–462.
- Morgante, A., 1998, Modeling of synthetic seismic sections in structurally complex areas: *Mem. Soc. Geol. It.*, **52**, 441–455.
- Morgante, A., Barchi, M. R., D'Offizi, S., Minelli, G., and Piali, G., 1998, The contribution of seismic modeling to the interpretation of the CROP-03 line: *Mem. Soc. Geol. It.*, **52**, 91–100.
- Özdenvar, T., McMechan, G., and Chaney, P., 1996, Simulation of complete seismic surveys for evaluation of experiment design and processing: *Geophysics*, **61**, 496–508.
- Piali, G., Barchi, M., and Minelli, G., Eds., 1998, Results of the CROP-03 deep seismic reflection profile: *Mem. Soc. Geol. It.*, **52**, 1–657.
- Ponziani, F., De Franco, R., Minelli, G., Biella, G., Federico, C., and Piali, G., 1995, Crustal shortening and duplication of the Moho in the northern Apennines: A view from seismic refraction data: *Tectonophysics*, **252**, 391–418.
- Priolo, E., 1999, 2-D spectral element simulation of destructive ground shaking in Catania (Italy): *J. Seismol.*, **3**, 289–309.
- Rabbel, W., and Gajewski, D., eds., 1999, *Seismic exploration of the deep continental crust*: Pure Appl. Geophys., **156**, 1–370.
- Rudnick, R. L., and Fountain, D. M., 1995, Nature and composition of the continental crust: A lower crustal perspective: *Rev. Geophys.*, **33**, No. 3, 267–309.
- Vai, G. B., 1994, Crustal evolution and basement elements in the Italian area: Palaeogeography and characterization: *Boll. Geof. Teor. Appl.*, **36**, 411–434.
- Yarnold, J. C., Johnson, R. A., and Sorensen, L. S., 1993, Identification of multiple generations of crosscutting “domino”-style faults: Insights from seismic modeling: *Tectonics*, **12**, 159–168.
- Zeng, X., and West, G. F., 1996, Reducing spurious diffractions in elastic wavefield calculations: *Geophysics*, **61**, 1436–1439.